Received: 22 November 2017 | Revised: 21 February 2018 | Accepted: 9 April 2018

DOI: 10.4218/etrij.2017-0286

ORIGINAL ARTICLE

WILEY ETRI Journal

Simplified approach for symbol error rate analysis of SC-FDMA scheme over Rayleigh fading channel

Vinay Kumar Trivedi[1] | **Madhusudan Kumar Sinha**[2] | **Preetam Kumar**[1]

[1]Department of Electrical Engineering, Indian Institute of Technology, Patna, India.

[2]Department of Electrical Engineering, Indian Institute of Technology, Madras, India.

Correspondence
Vinay Kumar Trivedi, Department of Electrical Engineering, Indian Institute of Technology, Patna, India.
Email: vinay.pee14@iitp.ac.in

In this paper, we present a comprehensive analytical study of the symbol error rate (SER) of single-carrier frequency-division multiple access (SC-FDMA) with zero-forcing frequency domain equalization (ZF-FDE) over a Rayleigh fading channel. SC-FDMA is considered as a potential waveform candidate for fifth-generation (5G) radio access networks (RANs). First, the N_C fold convolution of the noise distribution of an orthogonal frequency-division multiplexing (OFDM) system is computed for each value of the signal-to-noise ratio (SNR) in order to determine the noise distribution of the SC-FDMA system. N_C is the number of subcarriers assigned to a user or the size of the discrete Fourier transform (DFT) precoding. Here, we present a simple alternative method of calculating the SER by simplifying the N_C fold convolution using time and amplitude scaling properties. The effects of the N_C fold convolution and SNR over the computation of the SER of the SC-FDMA system has been separated out. As a result, the proposed approach only requires the computation of the N_C fold convolution once, and it is used for different values of SNR to calculate the SER of SC-FDMA systems.

KEYWORDS
BER, noise characterization, OFDMA, Rayleigh, SC–FDMA, SER, zero-forcing

1 | INTRODUCTION

Orthogonal frequency-division multiplexing (OFDM) is used primarily to protect against the detrimental effects of wireless multipath channels. By sampling the received signal at an optimum time, the receiver can avoid the intersymbol interference (ISI) caused by fading environments up to the length of the cyclic prefix (CP) being used [1,2]. Moreover, for this reason, the CP is chosen to be slightly longer than the maximum delay spread of the fading channel. To summarize the advantages, OFDM systems transmit multiple low-data-rate subcarriers, resistant to multipath, spectrally efficient, and the frequency-domain representation further simplifies the error correction at the receivers and reduces the complexities involved in multiple-input multiple-output (MIMO) implementation. OFDM also supports multiple users or multiaccess scheduling. The primary design criteria for an OFDM-based communication system are the maximum delay spread, maximum Doppler frequency, and the targeted cell size.

However, OFDM has two significant drawbacks. First, the high peak-to-average power ratio (PAPR) results in problems at the amplifiers. The other disadvantage is related to the tightly spaced subcarriers that are induced to compensate the loss of bandwidth due to CP insertion. The subcarriers start to lose orthogonality because of frequency errors [3]. Aside from the CP overhead and high sensitivity to frequency, the timing offset limits the performance of OFDM systems. The undesirable high PAPR of OFDM led the third generation partnership project (3GPP) to choose a different modulation format for the long-term evolution (LTE) uplink, namely the single-carrier frequency-division multiple access

(SC-FDMA) [4]. SC-FDMA is an extended version of single-carrier frequency domain equalization (SC-FDE), which allows multiple access [5], and it has enabled a very efficient power amplifier design for battery-operated handsets [6].

The potential of 5G wireless networks is expected to extend beyond the previous generations. These capabilities include high data rate, low latency, high reliability, low power consumption, and extremely high densities [7]. Currently, the goal is to fulfill these requirements using a combination of existing radio access LTE as well as additional advancements. It is probably that 5G will not be based on a particular radio access technology (RAT), but will incorporate several access and connectivity keys to address the previously mentioned requirements. One of the significant insights is to investigate the interoperability of existing LTE networks and the proposed 5G's new RAT, which is expected to impact communications and how businesses operate. Applications that will be supported by 5G mobile communications can be grouped into three major categories. These include enhanced mobile broadband services (eMBB), massive machine-type communication, and ultra-reliable and low-latency communication [8].

Waveform design is one of the critical aspects for defining the PHY and MAC layer for 5G mobile communications. An ideal waveform should have high spectral efficiency for high data rates, low PAPR allowing efficient power amplifier design, should enable mobility or robustness against Doppler shifts, and support asynchronous transmission and reception. Recently, in [9] and [10], the authors reported the potential for using the discrete-Fourier transform (DFT) spread OFDM as a potential 5G waveform candidate, with expected benefits being flexibility, spectrum, latency, and robustness to fading channels, where the overhead can be tuned with the frequency selectivity of the channel. Furthermore, in [9], it has been shown that with subcarrier wise processing, it is easy to extend MIMO support. Then, more recently, fractional Fourier transform-based SC-FDMA has been proposed to improve robustness to residual CFO [11]. To realize the full advantage of SC-FDMA systems, the PAPR should be minimized and the CFO should be compensated. In [12], a novel carrier interferometry spreading is proposed for SC-FDMA systems for power-hungry and reliable underwater communications in the uplink.

The performance evaluation and analysis of SER of SC-FDMA systems over fading environments have been actively studied by researchers in [13–16]. In [13], the error probabilities were analytically evaluated for the first time for both zero-forcing (ZF) and minimum mean-square error (MMSE) frequency-domain equalization (FDE) for SC-FDMA systems. However, the upper bound of SER is calculated by performing only numerical calculations. Later, in [17], the authors examined the SER performance for ZF and MMSE FDE under the assumptions of independence in the channel frequency response for subcarriers that are allocated to any user. Recently, in [15] and [16], the performance analysis of SC-FDMA was significantly enhanced by studying the effective noise after equalization in SC-FDMA systems. In [18], the authors extended the analysis over independent, but not necessarily identically distributed Nakagami-m fading channels with integer-fading parameters.

A popular approach deals with averaging the conditional SER with a Gaussian Q function [19] over the probability density function (PDF) of the instantaneous SNR per bit $f_\gamma(\gamma)$. Moreover, the Gaussian Q function depends on the modulation and detection techniques that are used [20]. As a major shortcoming, these types of methods generally do not result in closed-form SER expressions. Another prominent method is to calculate the moment-generating function (MGF) of the instantaneous SNR of the signal conditioned to the channel response [21]. It exploits from a simple finite-range integral, whose integrand consists only of an elementary function, and numerically calculates the SER with ease. In one of the approaches, assuming the independence among the frequency responses for allocated subcarriers allows us to obtain numerical expressions for the SER. This framework is very similar to that proposed in [22]. In this case, the SER can be calculated as

$$\mathrm{SER} = \sum_{n=1}^{L-1} w(n)\, I(n). \tag{1}$$

$I(n)$ are referred to as the components of the error probability (CEP) [22], and $w(n)$ are coefficients that are dependent on the symbol mapping used. The CEPs can be expressed as a function of the cumulative distribution function (CDF) that corresponds to the real part of the complex noise η affecting the symbol before the decision (F_{η_r}).

$$\begin{aligned} I(n) &= \Pr\{\Re(\eta) > (2n-1)d\} \\ &= 1 - F_{\eta_r}\left((2n-1)d\right) \end{aligned} \tag{2}$$

where d is the minimum distance between each symbol and decision boundary. For SER calculations, we first studied the stochastic behavior of complex noise after FDE, and we provided a platform to calculate the CDF of this complex noise. The resulting method will be simplified if the complex noise before the decision is circularly symmetric. Under these conditions, it is possible to find the noise distribution along the real and imaginary axis separately, and only then is one of its marginal distributions required. It is observed that for $N_C > 2$, the analytical framework presented in [15] becomes very complex, and there is no direct solution to the integral in (20). However, the possibility of complex inversion using the Gil-Peláez inversion formula [23] can be further considered, and the achievement of a good accuracy in the calculation of an integral with low computational cost requires that the upper limit $\omega_{\max}$ in (21) be selected carefully.

Our primary contribution is a comprehensive study of the approach in [15] to calculate the SER of SC-FDMA systems. We have proposed a simplified alternative method by simplifying the N_C fold convolution using the properties of convolution such as time and amplitude scaling. Using the proposed approach, we separated out the effect of the N_C fold convolution and SNR to calculate the SER. The proposed approach requires that the N_C fold convolution be determined by converting each individual noise distribution into the respective characteristic function (CHF) only once, and using the same result to calculate the SER for different values of SNR for SC-FDMA systems. The analysis that was presented has been verified using Monte Carlo simulations in MATLAB. Furthermore, our simplified mathematical approach gives consistent results, as in [15], for BPSK- and QPSK-modulated ZF-FDE SC-FDMA.

2 | SYSTEM MODEL

The transmitter and receiver schematic of SC-FDMA is given in Figure 1. SC-FDMA is considered as DFT-spread-OFDM because the DFT at the beginning spreads the modulation symbols over the subcarrier, and thus, every subcarrier possesses a portion of each modulated symbol. While doing so, fluctuations of the envelope of the transmitted waveform are considerably reduced. The PAPR is lowered but differs, and depends on the modulation used, and filtering is applied at the end of the signal processing chain at the transmitter.

For any given user, the collection of bits to be transmitted is mapped to the complex symbols (BPSK, QPSK, or M-QAM). The vector consisting of N_C complex symbols, x, is then mapped to an N_C point DFT. F represents the $N_C \times N_C$ DFT matrix, with the $(j,k)^{\text{th}}$ element being $\frac{1}{\sqrt{N_C}} e^{i\frac{2\pi}{N_C}jk}$ and $FF^H = I$. Let $x = [x_0, x_1, \ldots, x_{N_C}]$ be the data symbol to be transmitted. After N_C point DFT, we obtain $X_{N_C} = F.x$ in the frequency domain. This step is the main difference with OFDM, as complex symbols are now transmitted sequentially compared to parallel transmission in the case of OFDM. This actually results in the reduction of fluctuations in the overall envelope of the transmitted waveform. A subcarrier mapper assigns frequency-domain symbols to N_C available subcarriers out of M total subcarriers, in which the overall bandwidth is divided [5]. The transmitted signal vector X_{N_C} is then mapped to M orthogonal available subcarriers.

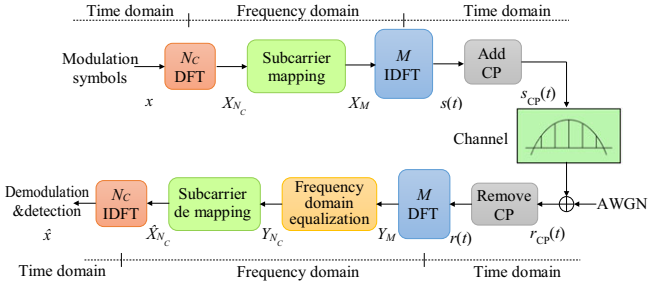

FIGURE 1 Single-carrier FDMA system schematic

$$X_M = C.X_{N_C} \tag{3}$$

where C is an $M \times N_C$ mapping matrix for which $C_{ij} = 1$ when symbol j is transmitted over subcarrier i; else, it is 0. The choice is to use localized mapping (i.e., LFDMA) or interleaved mapping (i.e., IFDMA) cum spectrum-distribution techniques to accommodate multiple users.

The paper considers only the IFDMA subcarrier assignment, which incurs a lower complexity cost in scheduling, and achieves a greater diversity gain as a large frequency spacing exists between the allocated subcarriers of any single user. The channel frequency response at each subcarrier is independent, as the coherence bandwidth is assumed to be small [14]. Furthermore, the transpose of the mapping matrix is a de-mapping matrix used at the receiver, or $CC^H = I_M$. In addition, the subcarriers used for different users should not overlap each other, ensuring that there is orthogonality among users.

$$C^k.\left(C^j\right)^T = \begin{cases} 0_M, & k \neq j; \\ I_M, & k = j. \end{cases} \tag{4}$$

Following the schematic of the SC-FDMA transmitter, an IFFT operation converts the frequency-domain symbols into the time domain, $s(t)$, and a CP is added to avoid ISI, $s_{\text{CP}}(t)$. The signal at the receiver end is the transmitted signal transformed by the channel response and contaminated by additive white Gaussian noise (AWGN), r_{CP}. After the CP suppression, the DFT converts each time-domain symbol into the frequency domain. After subcarrier demapping, the received signal is expressed as:

$$Y_{N_C} = C^H H_M C F x + C^H \eta_M \tag{5}$$

where η_M is the noise vector whose components are an independent and identically distributed (i.i.d.) Gaussian with mean zero and variance, N_0. H_M is an $M \times M$ diagonal channel matrix for the total number of subcarriers. Perfect estimation and synchronization have been assumed at the receiver. The recovered symbol after ZF-FDE and inverse precoding or N_C DFT is given by

$$\begin{aligned} \hat{x} &= F^H\left(H^H H\right)^{-1} H^H H\, F + F^H\left(H^H H\right)^{-1} H^H \eta \\ &= x + F^H\left(H^H H\right)^{-1} H^H \eta \end{aligned} \tag{6}$$

where $\eta = (C)^H \eta_M$ is a vector with elements corresponding to complex noise values, and $H = C^H H_M C$ is an $N_C \times N_C$ diagonal matrix whose coefficients are the channel response at each of N_C allocated subcarriers. The kth received symbol after ZF-FDE can be written as

$$\hat{x}_k = x_k + \sum_{j=1}^{N_C} \frac{F^*_{j,k}}{h_j}\eta_j = x_k + \sum_{j=1}^{N_C} \hat{\eta}_j = x_k + \tilde{\eta}_k \tag{7}$$

where $\hat{\eta}_j = \frac{F^*_{j,k}}{h_j}\eta_j$, and each received symbol adds an effective noise term to the transmitted symbol [13]. This effective noise exists because of the sum of the elementary noise term $\hat{\eta}_j$, or the enhanced Gaussian noise for each subcarrier in the OFDM system (noise in the OFDM with ZF-FDE).

3 | STATISTICAL CHARACTERIZATION OF NOISE AND SER ANALYSIS

The effective noise in an OFDM system is modeled as the ratio of the Gaussian noise distribution and Rayleigh fading coefficient [16].

$$\hat{\eta}_j = \frac{\eta_{\text{gaussian}}}{h_{\text{rayleigh}}} \tag{8}$$

where η_{gaussian} has a two-dimensional (2D) Gaussian distribution, and h_{rayleigh} has a Rayleigh distribution that is the magnitude distribution of a 2D Gaussian random variable. A 2D zero-mean Gaussian noise can be modeled as the magnitude and phase distribution, both independent of each other. Therefore, $\hat{\eta}_j$ has a magnitude distribution given by the ratio of two Rayleigh distributions, and has a uniform phase distribution in $[0, 2\pi]$ independent of the magnitude distribution.

To understand the derivation of the density function of $\hat{\eta}_j$ or $f_{\hat{\eta}_j}$, let X and Y be two Rayleigh random variables, and let Z be the ratio X/Y corresponding to the magnitude distribution of $\hat{\eta}_j$. X and Y are independent and continuous random variables with distribution $f_X(x)$ and $f_Y(y)$. Then, the distribution $f_Z(z)$ is given by

$$f_Z(z) = \int_{-\infty}^{+\infty} f_X(yz) f_Y(y)\, |y|\, dy. \tag{9}$$

Because $f_Y(y)$ is nonzero only for positive values of y, the above integral reduces to

$$f_Z(z) = \int_{0}^{+\infty} f_X(yz) f_Y(y)\, dy, \tag{10}$$

$$f_Z(z) = \frac{z}{\sigma_X^2 \sigma_Y^2} \int_{0}^{+\infty} y^3 e^{-\left(\frac{z^2}{2\sigma_X^2} + \frac{1}{2\sigma_Y^2}\right) y^2} dy \tag{11}$$

where σ_X^2 and σ_Y^2 are the respective variances of X and Y. Substituting $x^2 = t$ and then using integration by parts, we obtain:

$$f_Z(z) = \frac{2\sigma_X^2 \sigma_Y^2\, z}{\left(\sigma_X^2 + \sigma_Y^2\, z^2\right)^2}. \tag{12}$$

Because both X and Y have a uniform phase distribution over $[0,2\pi]$, the phase distribution $f_z(\theta_z)$ is uniform in $[0,2\pi]$. In addition, as θ_z and z are independent random variables, the density of the ratio is given by

$$f_{Z,\theta}(z,\theta) = \frac{1}{2\pi} \frac{2\sigma_X^2 \sigma_Y^2\, z}{\left(\sigma_X^2 + \sigma_Y^2\, z^2\right)^2}. \tag{13}$$

Again, with respect to the calculation of the density of $\hat{\eta}_j$ or $f_{\hat{\eta}_j}$, for a normalized channel response, $\sigma_Y^2 = 1$ and replacing σ_X^2 with σ for simplicity, we obtain

$$f_{\hat{\eta}_j}(r,\theta) = \frac{1}{\pi} \frac{\sigma^2 r}{\left(\sigma^2 + z^2\right)^2}. \tag{14}$$

Using the change in variables, the above equation can be transformed into a bivariate joint PDF for real and imaginary components of the elementary noise term, or enhanced Gaussian noise for each subcarrier in the OFDM system ($\hat{\eta}_j$)

$$f_{Re(\hat{\eta}_j), Im(\hat{\eta}_j)}(x,y) = \frac{1}{\pi} \frac{\sigma^2}{\left(\sigma^2 + (x^2 + y^2)\right)^2}. \tag{15}$$

The distribution in the above equation follows a Pearson-type VII family of distributions [24]. More specifically, it follows a Student t distribution with 2 degrees of freedom (DoFs), mean (0, 0), and scale matrix $\frac{\sigma^2}{2} I_2$, where I_2 is the identity matrix with size 2. From this result, we can separately find distributions along the real and imaginary axes. The marginal distribution of this Student t distribution follows the same distribution, which is given as

$$\begin{aligned} f_{Re(\hat{\eta}_j)}(x) &= \frac{1}{2} \frac{\sigma^2}{\left(\sigma^2 + x^2\right)^{3/2}}, \\ f_{Im(\hat{\eta}_j)}(y) &= \frac{1}{2} \frac{\sigma^2}{\left(\sigma^2 + y^2\right)^{3/2}}. \end{aligned} \tag{16}$$

As the joint PDF is circularly symmetric, the value of the distribution depends only on the radius of the circle on which the value lies. Therefore, the real and imaginary marginal densities are described by the same even function. As the complex noise before detection or enhanced noise is circularly symmetric, only one of its marginal distributions is actually required. For simplicity, we only considered $f_{Re(\hat{\eta}_j)}(x)$ and denoted it by $f_{(\hat{\eta}_j)}(x)$. The mean of this PDF is 0, and it has no finite variance, and thus, no MGF. Actually, these are long-tailed distributions with infinite moments [25]. The corresponding CDF of $\hat{\eta}_j$ is given as

$$F_{\hat{\eta}_j}(x) = \frac{1}{2} + \frac{x}{2\sqrt{\sigma^2 + x^2}}. \quad (17)$$

From here, it is numerically possible to calculate the SER expression of the binary phase-shift keying (BPSK) in OFDM over the Rayleigh channel, as in (1) and (2) [26]. The effective noise term before decoding is obtained by the inverse fast Fourier transform (IFFT) of N_C elementary noise terms with distribution given in (16). Because the elementary noise term at each subcarrier is circularly symmetric, the IFFT operation can be considered as the summation of N_C such terms. The effective noise can be modeled as the summation of N_C noise terms along the X and Y-axes. Now, because the distribution of the summation of random variables is given by the convolution of individual distributions,

$$\begin{aligned} f_{\tilde{\eta}_k}(x) &= f_{(\hat{\eta}_j)}(x) * f_{(\hat{\eta}_j)}(x) * \ldots N_C \quad \text{terms} \\ f_{\tilde{\eta}_k}(x) &= f^{*N_C}_{(\hat{\eta}_j)}(x) \end{aligned} \quad (18)$$

where $f^{*N_C}_{(\hat{\eta}_j)}(x)$ represents the N_C fold convolution of $f_{(\hat{\eta}_j)}(x)$. One method that is employed to compute the CDF of the effective noise in SC-FDMA, that is $\tilde{\eta}_k$, is to convert each individual noise distribution, that is, $f_{(\hat{\eta}_j)}(x)$, into a characteristic function $\Phi_{(\hat{\eta}_j)}(\omega)$ (CHF), as follows.

$$\begin{aligned} \Phi_{(\hat{\eta}_j)}(\omega) &= \int_{-\infty}^{\infty} f_{(\hat{\eta}_j)}(x)\, e^{j\omega\hat{\eta}_j} d\hat{\eta}_j \\ &= \sigma|\omega| K_1(\sigma|\omega|). \end{aligned} \quad (19)$$

This allows us to convert the convolution into multiplication in the frequency domain, as the CHF of the sum of the independent random variables is the product of their respective CHFs.

$$\begin{aligned} \Phi_{(\tilde{\eta}_k)}(\omega) &= \prod_{k=1}^{N_C} \Phi_{(\hat{\eta}_j)}(\omega) \\ &= (\sigma|\omega| K_1(\sigma|\omega|))^{N_C}. \end{aligned} \quad (20)$$

From (20), the distribution $f_{\tilde{\eta}_j}(x)$ can be calculated as

$$f_{\tilde{\eta}_k}(x) = \frac{1}{2\pi} \int_{-\infty}^{\infty} (\sigma|\omega| K_1(\sigma|\omega|))^{N_C} e^{-j\omega\tilde{\eta}_k} d\omega. \quad (21)$$

In general, this numerical integration is required to obtain the distribution $f_{\tilde{\eta}_k}(x)$, the associated CDF, and finally the SER using (1) and (2). However, it is only possible to calculate the analytical result of the above integral for $N_C = 2$, which also involves complex hypergeometric functions. There is no analytical solution of this integral for $N_C > 2$ in literature, but it is possible to obtain a more complex inversion theorem, which was proposed by Gil-Peláez [23] as follows.

$$F_{\tilde{\eta}_k}(x) = \frac{1}{2} + \frac{1}{2\pi} \int_0^{\infty} \frac{e^{ix\omega}\Phi_{(\tilde{\eta}_k)}(-\omega) - e^{-ix\omega}\Phi_{(\tilde{\eta}_k)}(\omega)}{i\omega} d\omega. \quad (22)$$

The above integral can be solved using the complex trapezoidal rule. Among the intervals of the above integral $\omega_{\min}$ is 0, whereas $\omega_{\max}$ should be carefully chosen to achieve good accuracy with low computational cost. The CHFs in the above integral $\Phi_{(\tilde{\eta}_k)}(\omega)$ are the symmetric exponential decaying function with a decay rate that is dependent on $\sigma|\omega|$. In fact, the decay rate is shown to be inversely proportional to SNR, and directly proportional to the number of allocated subcarriers or N_C .

In [15] and [16], the above approach was employed, where the CHF of $f_{(\hat{\eta}_j)}(x)$ is taken and raised to the power of N_C; the CDF is then calculated numerically to obtain the CEPs used to estimate the SER, as given in (1) and (2). Because the number of subcarriers allocated to a user (N_C) is of the order of 2^n, we need to compute n convolution operations, as in (18). By using some of the simple properties of convolution, such as the amplitude and time scaling, we can further simplify the calculation of $f_{(\hat{\eta}_j)}(x)$, which allows us to obtain directly approximately close-form SER expressions, which are validated using Monte- Carlo simulations in MATLAB.

The distribution of the effective noise in SC-FDMA is given by the N_C fold convolution of the elementary noise distributions obtained in (18).

$$f_{(\hat{\eta}_j)}(x) = \left[\frac{0.5\sigma^2}{(\sigma^2 + x^2)^{3/2}}\right]^{*N_C} = \left[\frac{1}{\sigma}\frac{0.5}{\left(1 + \left(\frac{x}{\sigma}\right)^2\right)^{3/2}}\right]^{*N_C}. \quad (23)$$

Using the amplitude scaling property of the convolution [27],

$$f_{(\hat{\eta}_j)}(x) = \frac{1}{\sigma^{N_C}} \left[\frac{0.5}{\left(1 + (x/\sigma)^2\right)^{3/2}}\right]^{*N_C}. \quad (24)$$

Let $C(x) = \left[\frac{0.5}{(1+x^2)^{3/2}}\right]^{*N_C}$. Using the time-scaling property of the convolution (i.e., $y(at) = |a|x(at) * h(at)$) [27],

$$f_{(\hat{\eta}_j)}(x) = \frac{1}{\sigma^{N_C}} \times \sigma^{(N_C - 1)} \times C\left(\frac{x}{\sigma}\right) = \frac{1}{\sigma} C\left(\frac{x}{\sigma}\right). \quad (25)$$

The CDF can be simply calculated using

$$F_{\tilde{\eta}_k}(x) = \int_{-\infty}^{x} \frac{1}{\sigma} C\left(\frac{x}{\sigma}\right) \mathrm{d}x = \int_{-\infty}^{x/\sigma} C(u) du. \quad (26)$$

The relation between the σ^2 used for OFDM systems and the SNR of SC-FDMA systems is given as $\sigma^2 = \frac{N_C}{\mathrm{SNR}}$. In addition, as $C(u)$ is an even-symmetric function:

$$F_{\tilde{\eta}_k}(x) = \int_{-\infty}^{\frac{x}{\sqrt{N_C/\mathrm{SNR}}}} C(u)du = 0.5 + \int_{0}^{\frac{x}{\sqrt{N_C/\mathrm{SNR}}}} C(u)du. \quad (27)$$

The SER for BPSK, quadrature phase-shift keying (QPSK), or quadrature amplitude modulation (QAM) modulation can now be further calculated using the approach in (1) and (2), as reported in [22]:

$$\begin{aligned} &\mathrm{SER} = \sum_{n=1}^{L-1} w(n)\, I(n), \\ &I(n) = \Pr\{\Re(\eta) > (2n-1)d\} = 1 - F_{\eta_r}((2n-1)d) \end{aligned} \quad (28)$$

where $w(n)$ is the coefficient that is dependent on constellation mapping, as given in [Lopez-Martinez], and d is the minimum distance between each symbol and decision boundary, which is given as $d = \sqrt{E_S}$ for BPSK and $\sqrt{\frac{3E_S}{2(M-1)}}$ for M-QAM. L is 2 (for BPSK) and $\sqrt{M}$ (for M-QAM). Here, we calculated the approximate closed-form expressions of SER for BPSK and QPSK modulation. A similar method will be used to calculate the SER of M-QAM for (M = 4, 8, 16, and so on). The SER can be calculated as

$$\begin{aligned} \mathrm{SER}_{\mathrm{BPSK}} &= 1 - \int_{-\infty}^{\frac{1}{\sqrt{N_C/\mathrm{SNR}}}} C(u)du \\ &= 0.5 - \int_{0}^{\frac{1}{\sqrt{N_C/\mathrm{SNR}}}} C(u)du. \end{aligned} \quad (29)$$

Similarly,

$$\mathrm{SER}_{\mathrm{QPSK}} = 1 - \left[0.5 + \int_{-\infty}^{\frac{1}{\sqrt{2N_C/\mathrm{SNR}}}} C(u)du\right]^2 \quad (30)$$

where $C(u) = \left[\frac{0.5}{\left(1+(u)^2\right)^{3/2}}\right]^{*N_C}$, which is the N_C fold convolution of a Student t distribution. The proposed approach can be extended to higher-order modulations, that is, 16-QAM, 64-QAM, and so on, by calculating d for different modulation formats in (28). The simplified evaluation of this N_C fold convolution can be performed using the approach in [15] by treating $C(u) = \left[\frac{0.5}{\left(1+(u)^2\right)^{3/2}}\right]^{*N_C}$ as a strictly even and circularly symmetric function of u, as in (21). This is because the N_C fold convolution of an even and circularly symmetric function $\left[\frac{0.5}{\left(1+(u)^2\right)^{3/2}}\right]$ is still even and circularly symmetric. From (29) and (30), it can be seen that the effects of the N_C fold convolution and SNR have been separated in order to compute the SER of SC-FDMA systems. The proposed approach is a simple and alternative approach that can be used to calculate the SER by simplifying the N_C fold convolution using time and amplitude scaling. The proposed approach is simplified as it only requires that we solve the N_C fold convolution once independent of SNR compared to multiple N_C fold convolution computations, as in [15] for different values of SNR.

4 | RESULTS

The probability of error expressions derived in (28) and (29) is validated using Monte Carlo simulations in MATLAB. For simulation purposes, BPSK and QPSK modulation formats were used, and of a total of *512* subcarriers, the number of subcarriers allocated to each user, that is, N_C is 16 here. This enables us to accommodate up to 32 users using LFDMA or IFDMA. In general, the ratio Q, which is, M/N_C is calculated as the bandwidth spreading factor for SC-FDMA scheme. SC-FDMA can accommodate up to Q orthogonal source signals with each source occupying N_C orthogonal subcarriers. Although SC-FDMA aims to assign a large number of subcarriers to a single user, we have selected the number of subcarriers assigned to a single user to be equal to 16 in order to verify the analysis completed in Section 3.

We considered a Rayleigh frequency-selective channel and ZF-FDE at the receiver. The detailed simulation parameters used for the Monte Carlo simulation in MATLAB are presented in Table 1.

Figure 2 shows the variation of the distribution of effective noise $f_{\tilde{\eta}_k}(x)$ with different values of the number of subcarriers per user (N_C). As the number of terms in the convolution increases, the curve flattens more, indicating a degraded SER performance, as shown in Figures 4 and 5. Similarly, Figure 3 presents the variation of $f_{\tilde{\eta}_k}(x)$ as the SNR increases from zero to 20 dB. A better SER performance with increasing SNR in Figures 4 and 5 is justified by an increasing peak and narrowing of the width of $f_{\tilde{\eta}_k}(x)$.

Figures 4 and 5 present the SER performance for BPSK and QPSK-modulated SC-FDMA over a Rayleigh fading channel. The mathematical SER derived from (29) and (30) perfectly matches with the simulation under similar conditions.

It has been observed that with an increasing value of N_C, the SER performance degrades as the number of terms

TABLE 1 Simulation parameters

Parameters	Specifications
Modulation	BPSK, QPSK
DFT precoder size (N_C)	16
Total number of subcarriers (M)	512
SC-FDMA input block size	16
Cyclic prefix length	20
Channel	Rayleigh frequency selective
Receiver	Zero-forcing FDE

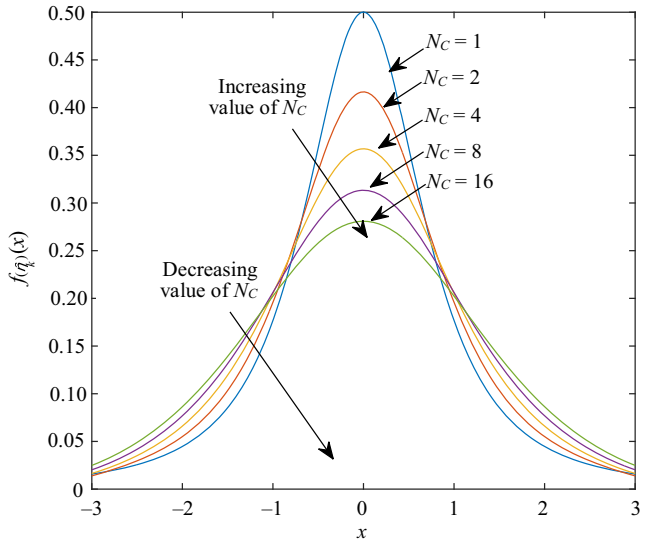

FIGURE 2 Behavior of effective noise $f_{\tilde{\eta}_k}(x)$ with different values of N_C

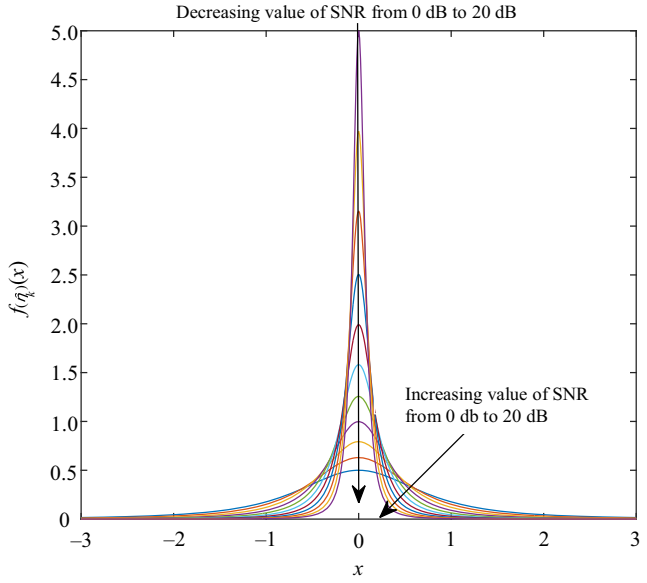

FIGURE 3 Behavior of effective noise $f_{\tilde{\eta}_k}(x)$ with different values of SNR

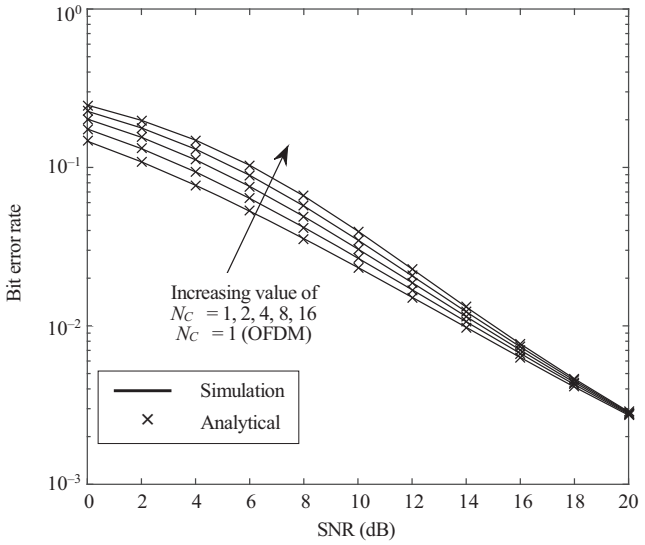

FIGURE 4 Analytical (29) vs simulated BER of SC-FDMA with BPSK modulation

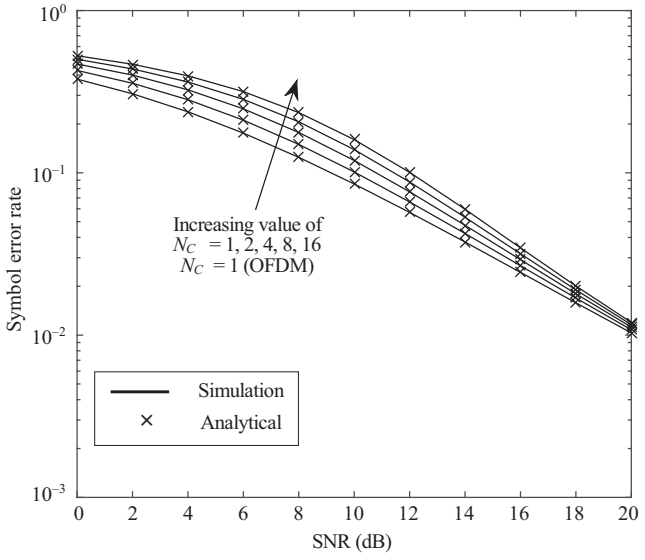

FIGURE 5 Analytical (30) vs simulated BER of SC-FDMA with QPSK modulation

in the convolution increases, and there is an increased probability of having a term close to zero in the channel frequency response. If we conditioned the effective noise to the channel frequency response, we see that it is a complex normal distribution $\sim C\left(0, \frac{N_0}{E_S}\beta_{ZF}\right)$, where $\beta_{ZF} = \frac{1}{N_C}\sum_{k=1}^{N_C}\frac{1}{|h_k|^2}$ is the zero-forcing noise-amplification factor introduced in [9]. The instantaneous SNR is now written as

$$\gamma = \frac{E_S}{N_0\beta_{ZF}} = \frac{E_S}{N_0}\frac{N_C}{\sum_{k=1}^{N_C}\frac{1}{|h_k|^2}}. \tag{31}$$

The above equation for the instantaneous SNR consists of the harmonic mean of random variables. Therefore, the computation of its moment-generating function (MGF) is a complex problem, and the SER cannot be calculated using the MGF approach [21]. The zero-forcing noise-amplification factor β_{ZF} is the sum of random variables with positive values, out of which any minimum value can serve as a lower bound of β_{ZF} given as $\beta_{ZF} > \frac{1}{N_C|h_{\min}|^2}$ and $\gamma < N_C|h_{\min}|^2\frac{E_S}{N_0}$. The value of the instantaneous SNR for $N_C > 1$ is always less when compared to OFDMA.

The effective SNR after ZF-FDE in SC-FDMA is always below that of OFDMA, which causes a rate loss. A

similar observation can be made for lower values of SNR, and the SER curves are always above OFDM with a difference that is increasing with increasing value of N_C or the number of allocated subcarriers to a user. Furthermore, as the SNR increases, all of the curves converge to an OFDM performance that is independent of N_C. This result is consistent with the fact that for ZF-FDE, OFDM has the lower bound for SER values of SC-FDMA.

5 | CONCLUSIONS

A comprehensive study of the numerical analysis of the error rate for SC-FDMA was observed over a Rayleigh fading channel with ZF-FDE. The proposed alternative approach that is employed to calculate the SER simplifies the N_C fold convolution using time and amplitude scaling properties of convolution. Moreover, we separated the effects of the N_C fold convolution and SNR to calculate the SER of SC-FDMA system. The result is an alternative simplified approach because it requires only a single computation of the N_C fold convolution, compared to multiple computations for different values of SNR. It was observed that in Rayleigh fading environments, the SER expressions for BPSK and QPSK follow the Monte Carlo simulations in MATLAB, and are in agreement with [15].

ORCID

Vinay Kumar Trivedi http://orcid.org/0000-0001-8796-7959

REFERENCES

1. G. L. Stuber et al., *Broadband MIMO-OFDM wireless communications*, Proc. IEEE **92** (2004), no.2, 271–294.
2. Z. Wang and G. B. Giannakis, *Wireless multicarrier communications*, IEEE Signal Process. Mag. **17** (2000), no. 3, 29–48.
3. S. Chen and C. Zhu, *ICI and ISI analysis and mitigation for OFDM systems with insufficient cyclic prefix in time-varying channels*, IEEE Trans. Consum. Electron. **50** (2004), no. 1, 78–83.
4. H. Ekstrom et al., *Technical solutions for the 3G long-term evolution*, IEEE Commun. Mag. **44** (2006), no. 3, 38–45.
5. H. Myung, J. Lim, and D. Goodman, *Single carrier FDMA for uplink wireless transmission*, IEEE Veh. Technol. Mag. **1** (2006), no. 3, 30–38.
6. H. Myung, J. Lim, and D. Goodman, Peak-to-average power ratio of single carrier FDMA signals with pulse shaping, in *2006 IEEE Int. Symp. Personal, Indoor Mobile Radio Commun.*, Helsinki, Finland, Sept. 11–14, 2006, pp. 1–5.
7. J. G. Andrews et al., *What will 5G be?*, IEEE J. Sel. Areas Commun. **32** (2014), no. 6, 1065–1082.
8. H.-S. Park et al., *LTE mobility enhancements for evolution into 5G*, ETRI J. **37** (2015), no. 6, 1065–1076.
9. G. Berardinelli et al., *Generalized DFT-spread-OFDM as 5G waveform*, IEEE Commun. Mag. **54** (2016), no. 11, 99–105.
10. A. Sahin et al., *Flexible DFT-S-OFDM: Solutions and challenges*, IEEE Commun. Mag. **54** (2016), no. 11, 106–112.
11. V. K. Trivedi and P. Kumar, FRFT-SCFDMA scheme for uplink in 5G radio access networks, in *IEEE Int. Conf. Commun. Workshops (ICC Workshops)*, Paris, France, May 21–25, 2017, pp. 785–790.
12. V. K. Trivedi and P. Kumar, *Carrier interferometry coded single carrier FDMA (CI/SC-FDMA) for next generation underwater acoustic communication*, Wireless Pers. Commun. **95** (2017), no. 4, 4747–4762.
13. M. D. Nisar, H. Nottensteiner, and T. Hindelang, On performance limits of DFT spread OFDM systems, in *IST mobile wireless communications*. Summit, Budapest, Hungary, July 1–5, 2007, pp. 1–4.
14. S. H. Song, G. L. Chen, and K. B. Letaief, *Localized or interleaved? A tradeoff between diversity and CFO interference in multipath channels*, IEEE Trans. Wireless Commun. **10** (2011), no. 9, 2829–2834.
15. J. J. Sanchez-Sanchez et al., Closed-form BER expression for interleaved SC-FDMA with M-QAM, in *IEEE Veh. Technol. Conf. Fall*, Anchorage, AK, USA, Sept. 20–23, 2009, pp. 1–5.
16. J. J. Sanchez-Sanchez, M. C. Aguayo-Torres, and U. Fernandez-Plazaola, *BER analysis for zero-forcing SC-FDMA over nakagami-m fading channels*, IEEE Trans. Veh. Technol. **60** (2011), no. 8, 4077–4081.
17. H. Wang et al., Performance analysis of frequency domain equalization in SC-FDMA systems, in *IEEE Int. Conf. Commun.*, Beijing, China, May 1–23, 2008, pp. 4342–4347.
18. M. Wen et al., *Error probability analysis of interleaved SC-FDMA systems over nakagami- m frequency-selective fading channels*, IEEE Trans. Veh. Technol., **62** (2013), no. 2, 748–761.
19. M. Abramowitz and I. A. Stegun, *Handbook of mathematical functions with formulas, graphs, and mathematical tables*, Tenth gpo. Dover printing: New York, USA, 1964.
20. M. K. Simon and M. S. Alouini, *Digital communication over fading channels*, Wiley-Interscience, Hoboken, NJ, USA, 2005.
21. M. K. Simon and M.-S. Alouini, *A unified approach to the probability of error for noncoherent and differentially coherent modulations over generalized fading channels*, IEEE Trans. Commun., **46** (1998), no. 12, 1625–1638.
22. F. J. López-Martínez et al., *Generalized BER analysis of QAM and its application to MRC under imperfect CSI and interference in Ricean fading channels*, IEEE Trans. Veh. Technol., **59** (2010), no. 5, pp. 2598–2604.
23. J. Gil-Peláez, *Note on the inversion theorem*, Biometrika, **38** (1951), 481–482.
24. K. Pearson, *Mathematical contributions to the theory of evolution. XIX. Second supplement to a memoir on skew variation*, Philos. Trans. R. Soc. A Math. Phys. Eng. Sci., **216** (1916), no. 538–548, 429–457.
25. M. G. Shayesteh and A. Aghamohammadi, *On the error probability of linearly modulated signals on frequency-flat Ricean, Rayleigh, and AWGN channels*, IEEE Trans. Commun. **43** (1995), no. 2/3/4, 1454–1466.

26. J. G. Proakis, *Digital communications*, 4th ed., McGraw-Hill, New York, USA, 2000.
27. R. K. R. Yarlagadda, *Analog and digital signals and systems*. Springer, Boston, MA, USA, 2010.

AUTHOR BIOGRAPHIES

Vinay Kumar Trivedi received the BEng degree in electronics and communication engineering from the Birla Institute of Technology Mesra, Ranchi, India, in 2013. He subsequently worked as an SAP Advanced Business Application Programming consultant at IBM from 2013 to 2014. He is currently working towards his PhD degree in the Department of Electrical Engineering, Indian Institute of Technology Patna, India. He is a Student Member of the IEEE. His current research interests include new waveforms and multiple-access radio technologies for 5G, underwater acoustic communications, and hybrid networks.

Madhusudan Kumar Sinha received the BTech degree in electronics and communication engineering from Bhagalpur Engineering College, Bihar, India, in 2013. He did his Masters in communication systems engineering from the Indian Institute of Technology Patna, India. He served as a Scientist-B for the National Institute of Electronics and Information Technology. He is currently pursuing his PhD from the Indian Institute of Technology Madras. His research areas include physical layer issues in wireless communications and 5G waveform design.

Preetam Kumar is currently working as an Associate Professor in the Department of Electrical Engineering, IIT Patna, India. He did his PhD from IIT Kharagpur in the area of wireless cellular communications in 2009. He was associated with the Birla Institute of Technology Mesra, Ranchi, from 2003 to 2009, before joining IIT Patna. He has a total of 18 years of teaching, research, and industry experience. His research interests include physical layer issues in wireless communications, error control coding, and digital communication systems. He has published several research papers in various refereed journals, including IEEE journals such as IEEE Communications Letters. He is a regular reviewer of premier journals, including the IEEE Transactions on Wireless Communications, Springer's Wireless Personal Communication Journal, as well as IEEE conferences such as ICC, GLOBECOM, VTC, WCNC, and PIMRC.